# Coupled THMC Processes in Radionuclide Waste Management

Gour-Tsyh (George) Yeh, CAMRDA
College of Earth Sciences, National Central University
No 300 Jhongda Road, Jhongli District, Taoyuan City 32001, Taiwan

Chia-Hsing (Peter) Tsai
Water Sciences and Management, 253 Skeen Hall, New Mexico State University
1780 East University Ave., Las Cruces, NM 88003

**Key words**; Multiphase Flow, Thermal Transport, Reactive Transport, Geo-Mechanics

**Abstract**

Physics-based mathematical-computational models provide an invaluable tool for repository design, performance/safety assessments, site clean-up, and environmental remediation in nuclear spent fuel and high level waste disposal in shallow or deep geological media. The migration of nuclear wastes is controlled by coupled THMC (Thermal-Hydrology-Mechanics-Chemical) processes. These include multiphase flow or variably saturated flow, thermal transport, reactive transport, and geo-mechanical deformation. Multiphase or variably saturated flow in subsurface media is the key driving mechanism for thermal transport, chemical transport, and geo-mechanics. Conversely thermal transport, chemical transport, and geo-mechanic deformation will affect flow directly or indirectly. Temperature changes are induced by fluid injection, associated phase changes, and chemical reactions. Conversely, temperature change will alter fluid flow, reactive transport, and geo-mechanical deformation. Faults and fractures will affect fluid pressure, thermal transport, and chemical migration. Conversely fluid pressure, thermal transport, and chemical migration will induce rock deformation and fault displacement. Reactive transport is controlled by fluid flow, affected by thermal transport, and influenced by geo-mechanical deformation. Conversely, reactive transport will have significant feedbacks on fluid flow, thermal transport, and geo-mechanics. This talk presents the development of a series of computational models that fully or partially couple these processes. Demonstrative applications are presented to illustrate the interplay of THMC processes and their implications for radionuclide waste managements.

## **1.** Introduction

The key issue in groundwater modeling is the ability to mathematically describe and numerically simulate coupled or decoupled physical, chemical, and biological processes, and their interactions with the media. The media include heterogeneous porous media and discrete fractures. The processes include fluid flow, thermal transport, reactive transport and bio-geochemistry, and geo-mechanical deformation. These are widely known as the THMC (Thermal, Hydrology or Hydraulics, geo-Mechanics, and reactive bio-geo-Chemistry) processes. Subsurface hydrology deals with flow in single or multi-fluid phases, including aqueous, super liquid, NAPL (non-aqueous phase liquid), gaseous phases, etc. Thermal transport deals with the evolution of temperature over the spatial domain. Reactive transport considers advection, dispersion, and diffusion of chemical species while they undergo biogeochemical reactions. Biogeochemical reactions include aqueous complexation, adsorption-desorption, ion-exchange, precipitation-dissolution, redox, acid-base reactions, microbial-mediated redox, the nutrient cycle, carbon cycle, metal cycle and biota kinetics. Geo-mechanics deals with the deformation or displacement of a solid skeleton.

The aforementioned THMC processes may be strongly or weakly coupled. Fluid flows are the key driving mechanism for thermal transport and bio-geo-chemical transport. The variations of pressure and degree of saturation in fluid phases may be a significant driving force in geo-mechanic deformation through the pressure force and gravity. In contrast, thermal transport, bio-geo-chemical transport, and geo-mechanic deformation may affect fluid flow. Temperature changes are induced by fluid injection, associated phase changes and chemical reactions. Conversely, temperature changes can affect fluid flow, reactive transport, and geo-mechanics. Reactive transport is controlled by fluid flow, as affected by media deformation and temperature changes. In contrast, reactive transport will have feedback to fluid flow, thermal transport, and geo-mechanical deformation. Geo-mechanically driven faults and fractures will affect fluid pressure, thermal transport, and chemical migration. Conversely fluid pressure changes, thermal transport, and bio-geo-chemical migration may induce rock deformation and fault displacement.

Table 1 lists some of the well-known and widely-used models that have included a single process or partially or fully coupled THMC processes. **Column 1** lists the model name, while **column 2** indicates what media these models can be applied to. Some models are applicable to only porous media (Macro), some are applicable to multi-porosity media (Macrco, Meso, and Micro), while others are applicable to porous media with embedded or imbedded fractures. **Column 3** indicates if flow processes are included. When these are included, some models are for saturated media (1P) only, some for variably saturated (VF), while some for multiple phase fluids (2P, 3P, or MP). There are basically two different ways to model multiphase flow: pressured-based (p-) and fractional flow-based (ff-) approaches. In general, fractional flow based approaches are more robust for numerical discretization. **Column 4** indicates if thermal transport is included in a model, while **Column 5** shows if a model has integrated commercially available solid mechanic models with other processes, or if geo-mechanics has been coupled with partial or full THC processes.

**Column 6** shows (1) the number of chemical components and the number of species in each component a model can handle, and (2) how components are determined. Some models can simulate the transport of Multiple Species (MS) without introducing the concept of components. Many models can simulate the transport of Multiple Components and each component includes Multiple Species (MCMS). A vast majority of models have pre-determined what the possible components are, and only a few can automatically determine components based on the input of reaction networks. However, those models that deal with multiple species might as well be said to deal with multiple components.

**Column 7** indicates how many THMC processes a model has been developed for, and these include H, C, C(R), HM, THM, THC, THC(R), THMC, and THMC(R). An H-model can only simulate flow processes. A C-model can only simulate solute transport or solute transport with adsorption of linear or nonlinear isotherms. A C(R)-model can simulate reactive chemical transport. An HM- model can simulate flow and mechanics. A THM-model can simulate thermal transport, flow, and mechanics. A THC- or THC(R)-model can simulate flow, thermal transport, and solute transport or reactive transport. A THMC- or THMC(R)-model has the capability to simulate all processes.

**Column 8** indicates what type of biogeochemical reactions a model can include. These reactions cover aqueous complexation (A/C), adsorption-desorption (A/D), ion exchange (I/E), precipitation-dissolution (P/D), and biological or microbe-mediated reactions (Bio). When a type of reaction is included, this column also shows if the reaction is treated as an equilibrium reaction (EQ), kinetic reaction (KI), or optional equilibrium or kinetic reaction (EK). For an

equilibrium reaction, a User Defined Algebraic equation (UDA) rather than the mass action equation may be used to implicitly define its rate. If a model allows UDA for all types of equilibrium reactions, it is labeled all (All). Column 8 also shows if a model allows Users to Define the Rate equation (UDR) for a kinetic reaction. If only biological reaction rates are allowed to be defined by users, it is labeled "Bio." If a model allows users to define rate equations for any type of kinetic reaction, it is labeled "All."

**Column 9** shows what Approach is employed to Couple Reactions and Transport (ACRT) in the reactive transport process. Basically, there are five popular approaches to coupling reactions and transport: the Direct Substitution Approach (DSA) or Global Implicit Method (GIM), Sequential Iteration Approach (SIA), Operator Splitting (OS), Predictor Corrector, and mixed Predictor Corrector and Operator Splitting (PC-OS). The advantages and disadvantages of these have been widely discussed in the literature. In general, the DSA or GIM will take too much CPU and RAM for large two- and three-dimensional problems, but they are perhaps the most accurate methods. The OS, PC, or PC-OS will take much less CPU than DSA or GIM, but are much less accurate. The SIA approach offers a compromise between these two previous kinds of approaches. Column 9 also shows what form of numerical discretization is adopted to discretize transport equations. These methods include Finite Element Methods (FEM), Finite Difference Methods (FDM) with Total Variation Diminishing (FDM/TVD) schemes for the advection transport, Integrated Finite Difference Methods (IFDM), Finite Volume Methods (FVM), and hybrid Lagrangian-Eulerian Finite Element Methods (LE-FEM). The LE-FEM methods and TVD are perhaps the methods to resolve the oscillation problems caused by advection transport.

Finally, **Column 10** indicates if a Mesh Generator (Mesh Gen) and Users Graphical Interface (GUI) are built into a model to facilitate its use with real-world problems.

## 2. Governing Equation of THMC models

It is believed that the best way to address the fully coupling issue of THMC processes is via the governing equations that are derived based on the principles of the conservation of mass, momentum, and energy. The explicitly coupled governing equations are given in the following subsections.

**2.1 Flow Equations.** The governing equations for multiphase flow are derived based on the conservation principle of phase mass and simplified momentum equations. The detailed derivations can be found elsewhere (Yeh and Tsai, 2015a, 2015b). Only the governing equations will be summarized in this paper. The governing equations of multiphase flow can be formulated using either the pressure-based or fractional flow-based approach.

***Pressure-Based Flow Equation*** The pressure-based governing equations of multiphase flow can be stated as follows (White and Oostrom, 1995; White et. Al., 1995; Xu and Pruess, 1998; Xu et al., 1998, 2003)

$$\begin{aligned}
&\phi S_\alpha \frac{\partial \hat{\rho}_\alpha}{\partial p_\alpha}\frac{dp_\alpha}{dt} + \phi \hat{\rho}_\alpha \frac{dS_\alpha}{dt} + \hat{\rho}_\alpha S_\alpha \frac{d\phi}{dt} + \phi S_\alpha \frac{\partial \hat{\rho}_\alpha}{\partial T}\frac{dT}{dt} \\
&\quad + \sum_{i\in\{M_\alpha\}} \phi S_\alpha \frac{\partial \hat{\rho}_\alpha}{\partial C_i^\alpha}\frac{dC_i^\alpha}{dt} + \phi \hat{\rho}_\alpha S_\alpha \frac{d(\nabla\cdot\mathbf{u})}{dt} = \\
&\nabla\cdot\left[\frac{\hat{\rho}_\alpha k_{r\alpha}}{\mu_\alpha}\mathbf{k}\cdot(\nabla p_\alpha + \rho_\alpha g \nabla z)\right] + M^\alpha + R^\alpha,\ \alpha\in\{L\}; \\
&\phi + \phi_s = 1;\ M^\alpha \equiv \sum_{i\in\{M_\alpha\}} M_i^\alpha,\ R^\alpha \equiv \sum_{i\in\{M_\alpha\}} R_i^\alpha;\ S_\alpha \equiv \frac{\phi_\alpha}{\phi}, \\
&\phi_\alpha \equiv \phi_{e\alpha} + \phi_{r\alpha},\ \phi_e \equiv \sum_{\alpha\in\{L\}} \phi_{e\alpha},\ \phi_r \equiv \sum_{\alpha\in\{L\}} \phi_{r\alpha},\ \phi \equiv \sum_{\alpha\in\{L\}} \phi_\alpha.
\end{aligned} \tag{2.1}$$

where $\phi$ is the porosity; $S_\alpha$ is the degree of saturation of Phase $\alpha$; $\hat{\rho}_\alpha$ is the molar density of Phase $\alpha$; $p_\alpha$ is the pressure of Phase $\alpha$; $t$ is the time; $T$ is the temperature; $\{M_\alpha\}$ having $M_\alpha$ members is the set index of all global species that are in Phase $\alpha$, where $M_\alpha$ is the number of species in Phase $\alpha$; $C_i^\alpha$ is the molar concentration of Species $i$ in Phase $\alpha$; $\mathbf{u}$ is the displacement; $k_{r\alpha}$ is the relative permeability of Phase $\alpha$; $\mu_\alpha$ is the dynamic viscosity of Phase $\alpha$; $\mathbf{k}$ is the intrinsic permeability tensor; $\rho_\alpha$ is the density of Phase $\alpha$; $g$ is the gravity constant; $z$ is the potential head; $M^\alpha$ is the artificial mass rate of Phase $\alpha$; $R^\alpha$ is the mass production rate of Phase $\alpha$ due to reactions; $\{L\}$ is equal to $\{1,2,\cdot\cdot,L\}$ in which $L$ is the number of fluid phases; $\phi_s$ is the volume fraction of the solid phase; $M_i^\alpha$ is the source/sink rate of Species $i$ in Phase $\alpha$; $R_i^\alpha$ is the production rate of Species $i$ in Phase $\alpha$ due to reactions; $\phi_\alpha$ is the porosity of Phase $\alpha$; $\phi_{e\alpha}$ is the effective porosity of Phase $\alpha$; $\phi_{r\alpha}$ is the residual porosity of Phase $\alpha$; $\phi_e$ is the effective porosity; and $\phi_r$ is the residual porosity.

The first and second equations in Eq. (2,1) consist of two equations involving 11 unknowns, $p_\alpha$, $\phi$; $S_\alpha$, $k_{r\alpha}$, $\hat{\rho}_\alpha$, $\rho_\alpha$; $T$; $C_i^\alpha$, $R_i^\alpha$; $\phi_s$ and $\mathbf{u}$. The temperature $T$ is governed by the thermal transport equation. The species concentrations $C_i^\alpha$ can be obtained from reactive transport equations, while $R_i^\alpha$ can be obtained via the biogeochemical reaction module. The solid phase volume fraction $\phi_s$ and displacement $\mathbf{u}$ are governed by the mass and

momentum conservation equations of solid phase in the geo-mechanic module. If we associate $p_\alpha$ and $\phi$ with the first and second equations in Eq. (2.1), we would need four more equations for four unknowns $S_\alpha$, $k_{r\alpha}$, $\hat{\rho}_\alpha$, and $\rho_\alpha$.

The densities $\hat{\rho}_\alpha$ and $\rho_\alpha$ are calculated using equations of states. In a reactive system, the equation of state for a phase should be derived based on the definition of phase density and the conservation of volume, as follows (Chang, 1995; Cheng, 1995; Yeh and Tsai, 2015a, 2015b)

$$\hat{\rho}_\alpha = \frac{\rho^\alpha_{maj}}{\cancel{M}^\alpha_{maj}} + \sum_{i\in\{M_\alpha\}, i\neq maj}\left(1-\frac{\cancel{M}_i}{\cancel{M}^\alpha_{maj}}\frac{\rho^\alpha_{maj}}{\rho^\alpha_i}\right)C^\alpha_i \quad \text{and}$$
$$\rho_\alpha = \rho^\alpha_{maj} + \sum_{i\in\{M_\alpha\}, i\neq maj}\left(1-\frac{\rho^\alpha_{maj}}{\rho^\alpha_i}\right)C^\alpha_i\cancel{M}_i,\ \alpha\in\{L\} \qquad (2.2)$$

where $\rho^\alpha_i\left(p^\alpha_i, T\right):\alpha\in\{L\}$, being function of partial phase pressure and temperature, is the intrinsic density of Species $i$ in Phase $\alpha$. It is noted that $\rho^\alpha_i = \rho^\alpha_i\left(p^\alpha_i, T\right)$ is in fact the equation of state for chemical species $i$ in phase $\alpha$. It is thus seen that the equation of state for a phase should be obtained from the equations of state of all chemical species in the phase in a reactive system. There are many specific forms of phase-based equations of state in reactive systems in the literature (e.g., Pruess, 1991; Finsterle et al., 1994; White and Oostrom, 1995; White et al., 1995).

The degree of saturation and relative permeability, $S_\alpha$ and $k_{r\alpha}$, are evaluated using K-S-P (Conductivity-Saturation-Pressure) constitutive laws, which are posed in general terms as follows

$$S_\alpha = S_\alpha\left(p_\alpha\right) \text{ and } k_{r\alpha} = k_{r\alpha}\left(p_\alpha\right),\ \alpha\in\{M_\alpha\} \qquad (2.3)$$

There are many specific forms of K-S-P equations in the literature (e.g., Burdine, 1953; van Genuchten, 1980; Parker et al, 1987a, 1987b; Lenhard and Parker, 1998; White and Oostrom, 1995; White et al., 1995; Yeh and Tsai, 2011; Tsai and Yeh, 2012, 2013).

The pressure-based multiphase flow equation is given in Eq. (2.1). This equation constitutes $L$ mixed parabolic and hyperbolic partial differential equations. The dominance of the hyperbolic or parabolic for each of $L$ equations varies over space and time. Furthermore, each equation is highly nonlinear. As a result, numerical solutions of these equations often encounter convergence difficulties. Furthermore, cumbersome procedures of variable switch have to be adapted to deal with phase disappearances.

***Fractional Flow-Based Flow Equation*** It is widely known that using a fractional-flow based approach could alleviate some of these problems (Allen, 1983; Abriola and Pinder, 1985a, 1985b; Guarnaccia and Pinder, 1997; Suck, 2003; Suk and Yeh, 2008), because such a method will produce one almost linear parabolic equation and $(L-1)$ hyperbolic-dominant equations. Hyperbolic-dominant equations can be ideally dealt with using hybrid Lagrangian-Eulerian numerical discretization (Yeh, 1990; Yeh, et al. 1995; Cheng et al., 1998; Suk and Yeh, 2007; Zhang et al., 2008). Phase disappearances were automatically taken care of (Suk and Yeh, 2007).

The fractional-flow based approach that originated in the petroleum engineering literature employs water saturation, total liquid saturation, and a total pressure as the primary variables for three-phase flow. For an arbitrary number of $L$ phases, the total pressure and $(L-1)$ accumulated effective degree of saturations can be employed as the primary variables. Detailed derivations of fractional-flow based governing equations for $L$ phases can be found elsewhere (Yeh and Tsai, 2015a, 2015b). In this paper, these equations are given as follows

$$S^P_{P_t}\frac{dP_t}{dt} + \sum_{t=1}^{L-1} S^P_{\tilde{S}_{tt}}\frac{d\tilde{S}_{tt}}{dt} + S^P_\phi\frac{d\phi}{dt} + S^P_T\frac{dT}{dt} + \sum_{\alpha=1}^{L}\sum_{i\in\{M_\alpha\}} S^P_{C^\alpha_i}\frac{dC^\alpha_i}{dt}$$
$$S^P_e\frac{d\left(\nabla\cdot\mathbf{u}\right)}{dt} = \nabla\cdot\left[\boldsymbol{\kappa}\cdot\left(\nabla P_t + \bar{\rho}g\nabla z\right)\right] + M^L + R^L$$
$$\text{in which } M^L \equiv \sum_{\alpha\in\{L\}} M^\alpha \text{ and } R^L \equiv \sum_{\alpha\in\{L\}} R^\alpha$$
$$S^\alpha_{P_t}\frac{dP_t}{dt} + \sum_{t=1}^{L-1} S^\alpha_{\tilde{S}_{tt}}\frac{d\tilde{S}_{tt}}{dt} + S^\alpha_\phi\frac{d\phi}{dt} + S^\alpha_T\frac{dT}{dt} + \sum_{i\in\{M_\alpha\}} S^\alpha_{C^\alpha_i}\frac{dC^\alpha_i}{dt} +$$
$$S^\alpha_e\frac{d\left(\nabla\cdot\mathbf{u}\right)}{dt} = \nabla\cdot\left(\kappa_\alpha\boldsymbol{\kappa}\cdot\nabla P_t\right) + \nabla\cdot\left[\kappa_\alpha\boldsymbol{\kappa}\cdot\left(\sum_{t=1}^{L-1} D^\alpha_{\tilde{S}_{tt}}\nabla\tilde{S}_{tt}\right)\right]$$
$$+\nabla\cdot\left(\kappa_\alpha\boldsymbol{\kappa}\cdot\rho_\alpha g\nabla z\right) + M^\alpha + R^\alpha,\ \alpha\in\{L-1\} \qquad (2.4)$$

in which

$$P_t = \frac{1}{L}\left(p_1 + p_2 + \ldots + p_{L-1} + p_L\right) +$$
$$\frac{1}{L}\sum_{\alpha=1}^{L-1}\int_0^{P_{c\alpha+1,\alpha}}\sum_{\gamma=\alpha+1}^{L}\sum_{\delta=1}^{\alpha}\left(\kappa_\gamma - \kappa_\delta\right)d\eta,\ p_{c\alpha+1,\alpha} = p_{\alpha+1} - p_\alpha;$$
$$\tilde{S}_{t\alpha} = \sum_{\beta=1}^{\beta=\alpha}\tilde{S}_\beta,\ \tilde{S}_\beta = \frac{\phi_\beta - \phi_{r\beta}}{\phi - \phi_r},\ \phi = \sum_\beta\phi_\beta \text{ for } \alpha\in\{L-1\};$$
$$\tilde{S}_{t0} = 0 \text{ and } \tilde{S}_{tL} = 1;\ \boldsymbol{\kappa} = \sum_{\beta=1}^{L}\frac{\hat{\rho}_\beta k_{r\beta}}{\mu_\beta}\mathbf{k};\ \tilde{\rho} = \sum_{\beta=1}^{L} S_\beta\hat{\rho}_\beta;$$
$$\bar{\rho} = \sum_{\beta=1}^{L}\kappa_\beta\rho_\beta;\ \text{and}\ \kappa_\alpha = \frac{\hat{\rho}_\alpha k_{r\alpha}}{\mu_\alpha}\Big/\sum_{\beta=1}^{L}\frac{\hat{\rho}_\beta k_{r\beta}}{\mu_\beta}. \qquad (2.5)$$

where $P_t$ is the total pressure, $\tilde{S}_{t\alpha}$ is the accumulated effective saturation up the $\alpha$-th phase, $\boldsymbol{\kappa}$ is the total mobility tensor, $\bar{\rho}$ is the mobility-weighted density, $M^L$ is the mass source/sink to all $L$ fluid phases, $R^L$ is the mass production rate in all $L$ fluid phases due to reactions, $\kappa_\alpha$ is the coefficient of fractional mobility for the $\alpha$-th phase, $D^\alpha_{\tilde{S}_{tt}}$ is the diffusion coefficient of the accumulated degree of saturation, $p_{c\alpha+1,\alpha}$ is the capillary pressure between the relative non-wetting phase $\alpha+1$ and wetting phase $\alpha$, $\tilde{S}_\beta$ is the effective degree of saturation of the $\beta$-th phase, and $\tilde{\rho}$ is the saturation-weighted molar density.

In Equation (2.4), $S_{P_t}^P$ and $S_{P_t}^\alpha$ are the storage coefficient of total pressure; $S_{\tilde{S}_{t\alpha}}^P$ and $S_{\tilde{S}_{t\alpha}}^\alpha$ are the storage coefficient of accumulated effective saturation; $S_\phi^P$ and $S_\phi^\alpha$ are the storage coefficient of porosity; $S_T^P$ and $S_T^\alpha$ are the storage coefficient of temperature; $S_{C_i^\alpha}^P$ and $S_{C_i^\alpha}^\alpha$ are the storage coefficient of species; and $S_e^P$ and $S_e^\alpha$ the storage coefficient of dilation. The superscript $^P$ in these storage coefficients denotes their appearance in the total pressure equation while the superscript $^\alpha$ denotes their appearance in the $\alpha$-th mass conservation equation.

**2.2 Thermal Transport Equation.** Assume thermal equilibrium in the system, the energy per phase volume can be related to the temperature via the specific capacity. In the meantime, the dispersive-diffusive-conductive heat flux is related to the gradient of temperature. Invoking the principle of energy conservation, we can derive the thermal transport equation as follows (Yeh and Tsai, 2015a, 2015b)

$$S_T\frac{dT}{dt}+K_TT+\nabla\cdot\left(\sum_{\alpha=1}^{L}\mathbf{V}_\alpha C_h^\alpha T\right)=\nabla\cdot\left[\left(\phi\sum_{\alpha=1}^{L}S_\alpha\left(\tilde{\mathbf{D}}_T^\alpha+\tilde{k}_T^\alpha\boldsymbol{\delta}\right)+\phi_s\tilde{\mathbf{k}}_T^s\right)\cdot\nabla T\right]+S_H^{out}+S_H^{in}+S_R \quad (2.6)$$

in which

$$S_T=\phi\sum_{\alpha=1}^{L}S_\alpha C_h^\alpha+\phi_sC_h^s,\ K_T=\frac{\partial S_T}{\partial t}+S_T\nabla\cdot\mathbf{V}_s,$$
$$S_R=-\sum_{k\in\{N\}}\Delta H_kr_k,\ \Delta H_k=\Delta H_k^oF(T)\ \text{with}\ \Delta H_k^o\ \&\ F(T)$$
$$\text{given by}\ \Delta H_k^o=\sum_{j\in\{M\}}\nu_{jk}\left(\Delta H_b^o\right)_j-\sum_{j\in\{M\}}\mu_{jk}\left(\Delta H_f^o\right)_j\ \&$$
$$F(T)=\exp\left[\frac{\Delta H_k^o}{R}\left(\frac{1}{T_o}-\frac{1}{T}\right)\right] \quad (2.7)$$

where $S_T$ is the storage coefficient of temperature; $K_T$ is the effective decay of the temperature; $\mathbf{V}_\alpha$ is the Darcy velocity of the fluid phase $\alpha$; $C_h^\alpha$ is the heat capacity of the fluid phase $\alpha$; $\tilde{\mathrm{D}}_T^\alpha$ is the apparent thermal dispersion coefficient tensor of the $\alpha$-th phase; $\tilde{k}_T^\alpha$ is the apparent thermal diffusion coefficient of the $\alpha$-th phase; $\tilde{\mathbf{k}}_T^s$ is the apparent thermal conductivity tensor of the solid phase; $S_H^{out}$ is the energy rate artificially taken out of the system; $S_H^{in}$ is the energy rate artificially injected into the system; $\mathbf{V}_s$ is the velocity of the solid skeleton; $S_R$ is the energy rate produced due to reactions; $\Delta H_k$ is the intrinsic reaction enthalpy of the $k$-th reaction; $\Delta H_k^o$ is the referenced reaction enthalpy of the $k$-th reaction; $\nu_{jk}$ is the stoichiometric coefficient of the product species $j$ in the $k$-th reaction; $F(T)$ is an empirical function of temperature; $\left(\Delta H_b^o\right)_j$ is the referenced formation enthalpy of the product species $j$; $\mu_{jk}$ is the stoichiometric coefficient of the reactant species $j$ in the $k$-th reaction; and $\left(\Delta H_f^o\right)_j$ is the referenced formation enthalpy of the reactant species $j$. It is noted that, similar to the Van't Hoff relationship for the equilibrium constant, we have used $F(T)=\exp\left[\Delta H_k^o\left(T-T_o\right)/\left(RTT_o\right)\right]$.

**2.3 Reactive Transport.** When the unit of species concentration is in moles per unit phase volume, the mass conservation equation for any chemical species is given as follows (Yeh and Tsai, 2015a, 2015b)

$$\frac{\partial\phi_\alpha C_i^\alpha}{\partial t}+\nabla\cdot\left(\mathbf{V}_\alpha C_i^\alpha\right)+\nabla\cdot\left(\phi_\alpha\mathbf{V}_sC_i^\alpha\right)=\nabla\cdot\left[\hat{\rho}_\alpha\phi_\alpha\left(\mathbf{D}_\alpha+\tau_\alpha a_m^\alpha\boldsymbol{\delta}\right)\cdot\nabla\chi_i^\alpha\right]+M_i^\alpha+R_i^\alpha,\ i\in\{M_\alpha\},\alpha\in\{L\};$$
$$\phi S_\alpha\mathbf{D}_\alpha=a_T^\alpha|\mathbf{V}_\alpha|\boldsymbol{\delta}+\left(a_L^\alpha-a_T^\alpha\right)\mathbf{V}_\alpha\mathbf{V}_\alpha/|\mathbf{V}_\alpha|;$$
$$\frac{\partial\phi_sC_i^s}{\partial t}+\nabla\cdot\left(\phi_s\mathbf{V}_sC_i^s\right)=\nabla\cdot\left(\hat{\rho}_s\phi_sa_m^s\boldsymbol{\delta}\cdot\nabla\chi_i^s\right)+R_i^s,\ i\in\{M_s\}. \quad (2.8)$$

where $C_i^\alpha$ is the molar concentration of Species $i$ in Phase $\alpha$; $\mathbf{D}_\alpha$ is the dispersion coefficient tensor for all species in the $\alpha$-th phase; $\tau_\alpha$ is the tortuosity for Phase $\alpha$; $a_m^\alpha$ is the molecular diffusion coefficient of all species in the $\alpha$-th phase; $\boldsymbol{\delta}$ is the Kronecker delta tensor; $\chi_i^\alpha$ is the mole fraction Species $i$ in Phase $\alpha$; $a_L^\alpha$ is the longitudinal diffusivity for Phase $\alpha$; $a_T^\alpha$ is the transverse diffusivity for Phase $\alpha$; $C_i^s$ is the molar concentration of Species $i$ in the solid phase; $\hat{\rho}_s$ is the molar density of the solid phase; $a_m^s$ is the molecular diffusion coefficient of all species in the solid; $\chi_i^s$ is the mole fraction Species $i$ in the solid phase; $R_i^s$ is the production rate of the solid species $i$ due to reactions; and $\{M_s\}$ having $M_s$ member is the set index of all global species that are in the solid phase, where $M_s$ is the number of species in the solid phase.

A reaction-based formulation would result in the following equation for $R_i^\alpha$ and/or $R_i^s$ as follows

$$R_i^\alpha=\sum_{k\in\{N\}}\left(\nu_{ik}-\mu_{ik}\right)r_k,\ i\in\{M\},\ \alpha\in\{L+1\} \quad (2.9)$$

in which

$$r_k=f_k\left(\breve{C}_i^\alpha:i\in\{M\},\alpha\in\{L+1\}\right),\ k\in\{N_K\}.$$
$$r_k:\leftarrow F_k\left(\breve{C}_i^\alpha:i\in\{M\},\alpha\in\{L+1\}\right)=0,\ \text{for example,}$$
$$\beta_k^e-\prod_{i\in M}\left(\breve{C}_i^\alpha\right)^{\nu_{ik}}/\prod_{i\in M}\left(\breve{C}_i^\alpha\right)^{\mu_{ik}}=0,\ k\in\{N_E\}.$$
$$\breve{C}_i^\alpha\ \text{is related to}\ C_i^\alpha\ \text{by}\ C_i^\alpha=\breve{M}_i\breve{C}_i^\alpha. \quad (2.10)$$

where $r_k$ is the rate of the $k$-th reaction; $\breve{C}_i^\alpha$ is the molality of the $k$-th species; $\{N_K\}$ having $N_K$ members is the set index of kinetic reactions; $\beta_k^e$ is the modified equilibrium constant of the $k$-th reaction; and $\{N_E\}$ having $N_E$ members is the set index of independent equilibrium reactions. Note: $\alpha = L+1$ denotes the solid phase; $N = N_E + N_K$.

Equations (2.8) through (2.9) constitute a system of $M$ transport equations and $N_E$ nonlinear algebraic equations for $M$ $C_i$'s and $N_E$ $r_k$'s of unknowns, after $N_K$ $r_k$'s in Eq. (2.10) is substituted into Eq. (2.8). Simultaneous solutions of this system of $M$ reactive transport equations and $N_E$ nonlinear algebraic equations over the entire domain of interest would demand excessive computational time and computer storage (Yeh and Tripathi, 1989), even with today's computers. Decoupling of the $N_E$ $r_k$'s of unknowns from the $M$ $C_i$'s of unknowns can be done via the Gauss-Jordan reduction of reaction networks (Chilakapati, et al., 1998; Fang, et al., 2003; Kräutle and Knabner, 2007). Performing the Gauss-Jordan reduction of reaction networks, we obtain

$$\frac{dE_i}{dt} + \nabla\cdot\left(\mathbf{V}_{E_i}E_i\right) + \frac{d\left(\nabla\cdot\mathbf{u}\right)}{dt}E_i = \nabla\cdot\left(\mathbf{D}_{E_i}\cdot\nabla E_i\right) + S_{E_i}^{ss} + R_{E_i},\ i\in\{M_C\}\cup\{M_{KI}\} \tag{2.11}$$

in which

$$E_i = \sum_{j\in\{M\}} a_{ij}\phi_\alpha C_j^\alpha,\ E_i^\alpha = \sum_{j\in\{M_\alpha\}} a_{ij}\phi_\alpha C_j^\alpha,$$
$$\mathbf{V}_{E_i} = \sum_{\alpha\in\{L\}}\left(\frac{\mathbf{V}_\alpha E_i^\alpha}{\phi_\alpha E_i} - \hat{\rho}_\alpha\phi S_\alpha\mathbf{D}_\alpha\cdot\nabla\frac{E^\alpha}{\hat{\rho}_\alpha\phi_\alpha E}\right) - \hat{\rho}_s\phi_s a_m^s\boldsymbol{\delta}\cdot\nabla\frac{E_i^s}{\hat{\rho}_s\phi_s E_i},$$
$$\mathbf{D}_{E_i} = \sum_{\alpha\in\{L\}}\frac{E_i^\alpha}{E_i}\mathbf{D}_\alpha + \frac{E_i^s a_m^s}{E_i}\boldsymbol{\delta},\ S_{E_i}^{ss} = \sum_{j\in\{M\}} a_{ij}M_j^\alpha,\ \text{and}$$
$$R_{E_i} = D_{ik}r_k + \sum_{j\in\{N_{KD(k)}\}} D_{ij}r_j \tag{2.12}$$

where $E_i$ is the $i$-th transformed variable; $\mathbf{V}_{E_i}$ is the advection velocity of $E_i$, $\mathbf{D}_{E_i}$ is the dispersion-diffusion coefficient tensor of $E_i$, $S_{E_i}^{ss}$ is the artificial source/sink rate contributing to the change of $E_i$; $R_{E_i}$ is the production rate of $E_i$ due to reactions, $\{M_C\}$ is the set index of components, $\{M_{KI}\}$ is the set index of kinetic variables, $a_{ij}$ is the decomposed unit matrix, $E_i^a$ is the content of $E_i$ in the $\alpha$-th phase, $E_i^s$ is the content of $E_i$ in the solid phase, $D_{ik}$ is the $i$-th row $k$-th column of the decomposed reaction matrix, and $\{N_{KD(k)}\}$ is the set index of kinetic reactions that are linearly dependent on the independent kinetic reaction $k$.

**2.4 Geo-Mechanic Equations.** The governing equations for the geo-mechanic module are obtained based on the conservation of mass and momentum as follows (Liu, 2002, 2006, 2011; Liu et al., 2010; Yeh and Tsai, 2015a, 2015b)

$$\left(\hat{\rho}_s + \phi_s\frac{\partial\hat{\rho}_s}{\partial p_s}\frac{dp_s}{d\phi_s}\right)\frac{d\phi_s}{dt} + \phi_s\frac{\partial\hat{\rho}_s}{\partial T}\frac{dT}{dt} + \sum_{i\in\{M_s\}}\phi_s\frac{\partial\hat{\rho}_s}{\partial C_i^s}\frac{dC_i^s}{dt} + \hat{\rho}_s\phi_s\frac{d\left(\nabla\cdot\mathbf{u}\right)}{dt} = R^s \quad \text{in which } R^s = \sum_{i\in\{M_s\}} R_i^s \tag{2.13}$$

and

$$\phi_s\rho_s\frac{d^2\mathbf{u}}{dt^2} \approx 0 = \nabla\cdot\mathbf{T} - \sum_{\alpha\in\{L\}}\nabla\left(S_\alpha p_\alpha\right) + \left[\sum_{\alpha\in\{L\}}\rho_\alpha\phi S_\alpha + \phi_s\rho_s\right]g\nabla z - \beta_T^g\nabla T - \sum_{i\in\{M_s\}}\beta_i^s\nabla C_i^s + \sum_{\alpha\in\{L\}}\sum_{i\in\{M_\alpha\}}\beta_i^\alpha\nabla C_i^\alpha \tag{2.14}$$

in which

$$\mathbf{T} = -\phi_s p_s\mathbf{I} + s_1\mathbf{B} + s_2\mathbf{B}^{-1} + \lambda(tr\mathbf{D})\mathbf{I} + 2\mu_1\mathbf{D} + \mu_2(\mathbf{DB}+\mathbf{BD}) + \mu_3(\mathbf{DB}^{-1}+\mathbf{B}^{-1}\mathbf{D})$$
$$\text{in which } \mathbf{B} = \mathbf{F}\mathbf{F}^T,\ \mathbf{F} = \mathbf{I}+\mathbf{H},\ \mathbf{H} = \nabla\mathbf{u},$$
$$\mathbf{D} = \frac{1}{2}\left(\dot{\mathbf{H}}+\dot{\mathbf{H}}^T\right),\ \text{and } \dot{\mathbf{H}} = \nabla\dot{\mathbf{u}} = \nabla\mathbf{V}_s \tag{2.15}$$

where $p_s$ is the solid phase pressure; $R_s$ is the mass production rate in the solid phase due to reactions; $\mathbf{T}$ is the is the Cauchy stress tensor (positive for tension) exerted on the medium; $\beta_T^g$ is the thermal expansion coefficient in the geo-mechanical module; $\beta_i^s$ is the expansion coefficient of the solid species concentration $C_i^s$; $\beta_i^\alpha$ is the expansion coefficient of the $\alpha$-th species concentration $C_i^\alpha$; $s_1$, $s_2$, $\lambda$, $\mu_1$, $\mu_2$, and $\mu_3$ are six model parameters, respectively; $\mathbf{F} = \nabla_{\mathbf{X}}x$ is the gradient of the deformation $x \equiv \mathbf{x}$ in the material frame $X \equiv \mathbf{X}$; $\mathbf{H} = \nabla_X\mathbf{u}$ is the gradient of the displacement $\mathbf{u}$ in the material frame $\mathbf{X}$; and $\dot{\mathbf{H}} = \nabla_X\dot{\mathbf{u}} = \nabla\mathbf{V}_s$ is the gradient of the solid phase velocity in the material frame $\mathbf{X}$.

Equations (2.13) through (2.15) consist of three equations involving 5 unknowns, $p_s$, $\phi_s$, and $\rho_s$ as well as $\mathbf{u}$ and $\mathbf{T}$. If we associate $\phi_s$, $\mathbf{u}$, and $\mathbf{T}$, respectively, with Eqs. (2.13), (2.14), and (2.15), respectively, we would need two more equations for two unknowns $\hat{\rho}_\alpha$ and $p_s$. The density $\hat{\rho}_s$ is calculated using the equation of state similar to those for fluid phases as follows(Chang, 1995; Yeh and Tsai, 2015a, 2015b)

$$\rho_s = \rho_{maj}^s + \sum_{i\in\{M_s\},i\neq maj}\left(1-\frac{\rho_{maj}^s}{\rho_i^s}\right)C_i^s\cancel{M_i} \tag{2.16}$$

where $\rho_i^s\left(p_i^s, T\right)$, being function of partial phase pressure and temperature, is the intrinsic density of Species $i$ in the solid phase. It is noted that

$\rho_i^s = \rho_i^s\left(p_i^s, T\right)$ is in fact the equation of state for chemical species $i$ in the solid phase. The constitutive equation of the solid phase pressure versus volume fraction of solid may be established as

$$p_s = f(\phi_s) \text{ in general, e.g., } p_s = p_{so} - \frac{1}{\alpha}\ell n\left(\frac{1-\phi_s}{1-\phi_{so}}\right) \quad (2.17)$$

## 3. A Demonstrative Example of THMC Modeling

This example is to demonstrate the capability of HYDROGEOCHEM 6.1 (Yeh and Tsai, 2015a) to simulate fully coupled THMC processes. Radioactive wastewater containing a high concentration of $NpO_2^+$ is injected into the media filled with a three-fluid phase (water, NAPL, and air) system (**Figure 1**). The media contains Region B with a zero adsorption site, $TOT_{SOH} = 0$, and Region A with a relatively high adsorption site, $TOT_{SOH} = 10^{-4}$ $mol\ d^3l$.

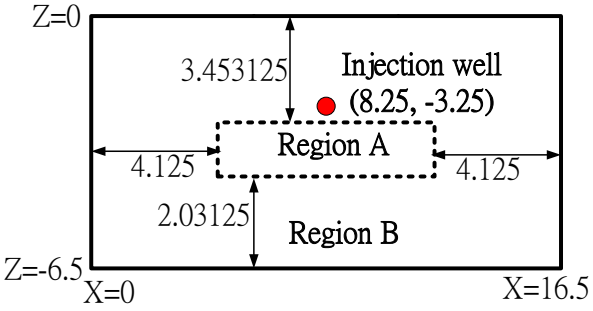


**Figure 1** Region of Interest and Location of Injection Well

For this problem a three-phase flow is considered, and thermal effects are included. Injection effects on geo-mechanics (porosity change and deformation) are also considered, while the chemistry includes both intra (homogeneous) and inter phase (heterogeneous) reactions. The initial and boundary conditions for flow simulation are depicted in **Figure 2**. The initial degree of saturation for aqueous, NAPL, and gaseous phases, respectively, are 0.1, 0.1, and 0.8 at boundary B4, and vary with a slope of 0.121212 % until they reach boundary B2. While the degrees of saturation will change due to a 0.1 $dm^3$ $day^{-1}$ of water injection rate, the degrees of saturation on all four boundaries are kept the same as the initial conditions.

In order to model thermal transport, the initial temperature is set at 298 $^oK$. The temperatures on four boundary sides are maintained at 298 $^oK$, while that in the injection well is 308 $^oK$ **(Figure 3).**

For reactive chemical transport, a reaction network consisting of 28 reactions involving 42 species is conceptualized, as shown in **Table 2**.

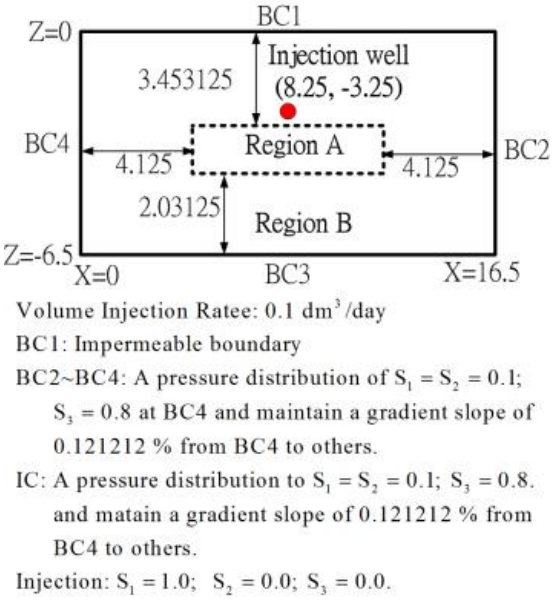


**Figure 2** Initial and Boundary Conditions and Artificial Source for Flow Simulation

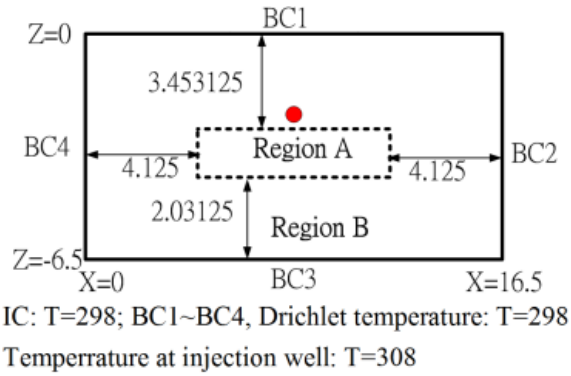


**Figure 3** Initial and Boundary Conditions and Artificial Source for Thermal Transport

The initial and boundary conditions for this hypothetical simulation of reactive transport are depicted in **Figure 4**. The initial and boundary conditions for three major species, $H_2O$, NAPL, and Air, are identical, and the same is true for the species $O_{(g)}$, $OH_{(g)}$, $CH_{4(g)}$, and $HCO_{(g)}$. The initial and boundary conditions for two aqueous components $Ca^{2+}$ and $CO_3^{2-}$ are also identical. The major disturbances to the reactive system are due to the injection of a high concentration of $NpO_2^+$, high initial concentration of $NpO_2^+$ in Region A, as well as high adsorption site in Region A.

For the geo-mechanical simulation (**Figure 5**), it is initially assumed there is no displacement throughout the region of interest. On boundary BC1, no external force is applied. On boundaries BC2 and BC4, it is assumed that the displacement in the horizontal direction and force in the vertical direction are zero, as depicted with rollers on these two boundaries. On

boundary BC3, vertical displacement is not allowed and the horizontal force acting on the surface is zero, which is represented by rollers attached to the

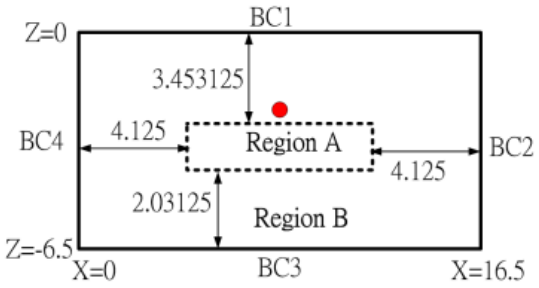


BC1~BC4 (Variable BC):

$Ca^{2+} = 1\times10^{-3}$; $CO_3^{2-} = 2\times10^{-3}$; $NpO_2^{+} = 1\times10^{-12}$; $H^{+} = 1\times10^{-5}$

IC (Region A): $Ca^{2+} = 1\times10^{-3}$; $CO_3^{2-} = 2\times10^{-3}$; $NpO_2^{+} = 1\times10^{-5}$; $H^{+} = 1\times10^{-5}$; $SOH = 4\times10^{-4}$

IC (Region B): $Ca^{2+} = 1\times10^{-3}$; $CO_3^{2-} = 2\times10^{-3}$; $NpO_2^{+} = 1\times10^{-12}$; $H^{+} = 1\times10^{-5}$; $SOH = 0$

Injection Well: $Ca^{2+} = 1\times10^{-3}$; $CO_3^{2-} = 2\times10^{-3}$; $NpO_2^{+} = 1\times10^{-5}$; $H^{+} = 1\times10^{-5}$

IC and BC: $H_2O = 55.56$; $NAPL = 6.06$; $AIR = 34.52$

$O(g) = 10^{-2}$; $OH(g) = 10^{-3}$; $CH_4(g) = 10^{-7}$; $HCO(g) = 10^{-7}$

**Figure 4** IC & BC for Reactive Transport

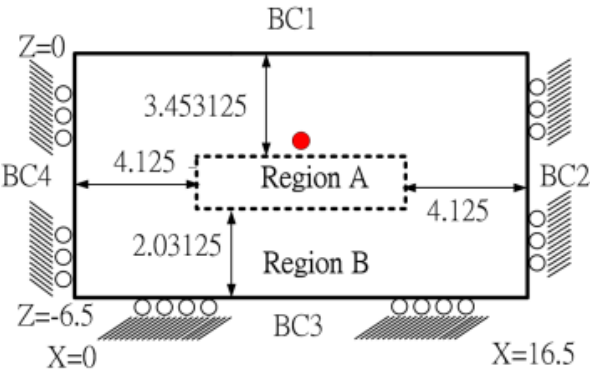


BC1: No external force, $\mathbf{F} = 0$; BC2, BC4: $u_x = 0$, $F_z = 0$

BC3: $u_z = 0$, $F_x = 0$; IC: $\mathbf{u} = 0$

**Figure 5** IC and BC for Geo-Mechanics

For numerical simulations with HGC 6.0 (Yeh and Tsai, 2013; Tsai and Yeh, 2014), a uniform mesh of 45 x 333 =1,485 nodes and 44 x 32 = 1,408 elements is used (**Figure 6**). The total simulation time is 2.985 days. The initial time step size is 0.0001 day. The maximum time step size is 0.001 day, and total number of time steps is 3,000.

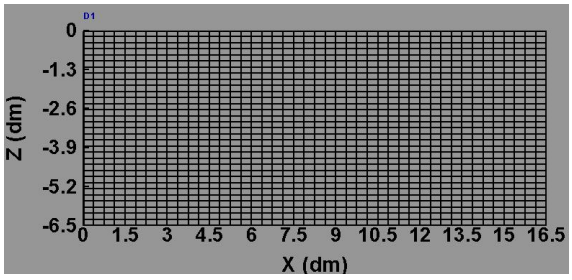


**Figure 6** FE Mesh: 1,408 Elements 1,485 Nodes

It is seen that water entering into the simulation region displaces the two other fluids (**Figure 7**). It is also seen that NAPL is displaced by the injection water and moves downward (**Figure 8**). On the other hand, air is displaced by the injected water and moves upward (**Figure 9**). These interactions among fluid phases are easily seen in **Figure 10**, where the stream lines and velocity vectors are shown.

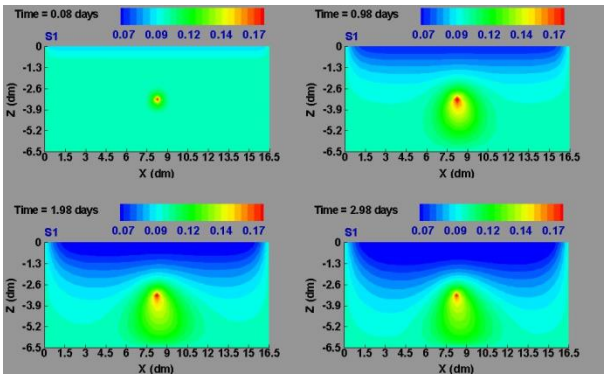


**Figure 7** Distribution of Degree of Saturation at Various Times for the Aqueous Phase

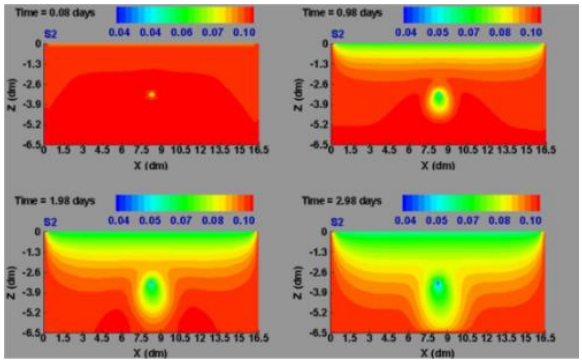


**Figure 8** Distribution of Degree of Saturation at Various Times for the NAPL Phase

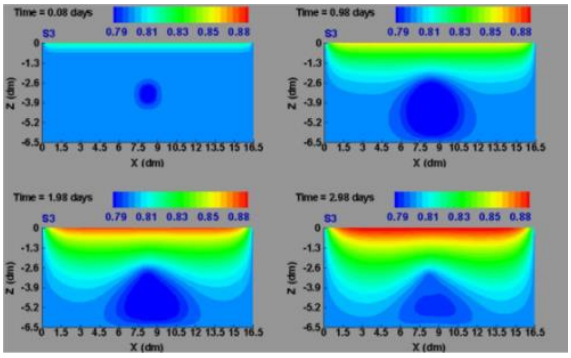


**Figure 9** Distribution of Degree of Saturation at Various Times for the Gaseous Phase

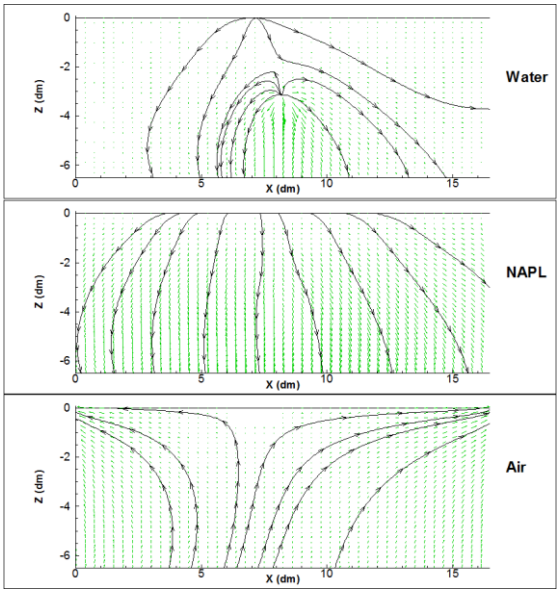


**Figure 10** Velocity Field at Time = 2.98 Days

Temperature decreases with the distance from the injection well and exhibits a non-symmetrical plume toward the right-upper direction (**Figure 11**). This behavior is caused by the non-symmetrical stream lines shown in Figure 10.

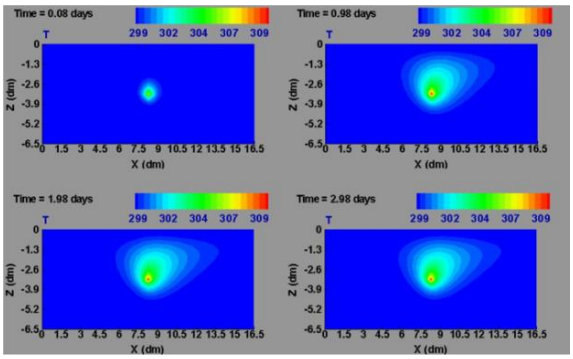


**Figure 11** Distribution of Temperature at Various Times

The total dissolved $NpO_2^+$ in all three phases is transported away from the injected well and retarded when reaching the adsorption region (**Figures 12, 13, and 14**).

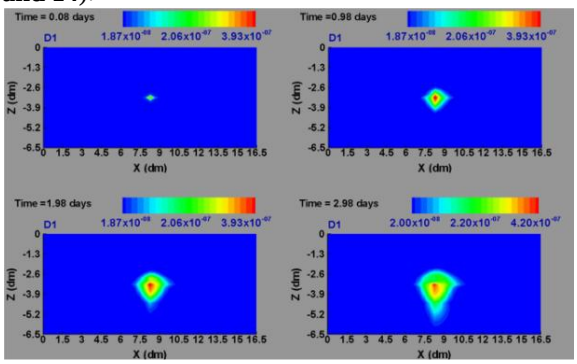


**Figure 12** Distribution of Total Dissolved $NpO_2^+$ in the Aqueous Phase at Various Times

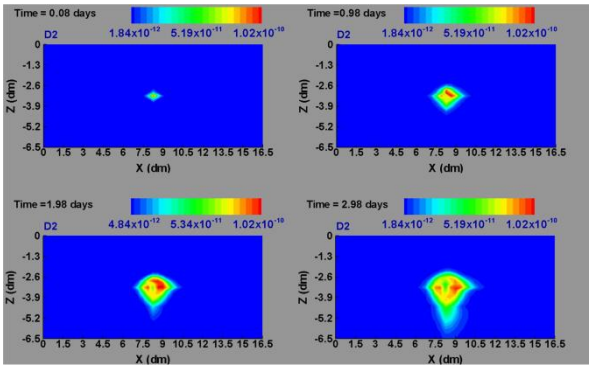


**Figure 13** Distribution of Total Dissolved $NpO_2^+$ in the NAPL Phase at Various Times

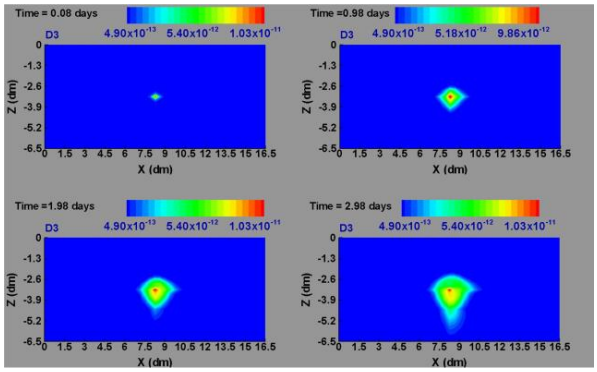


**Figure 14** Distribution of Total Dissolved $NpO_2^+$ in the Gaseous Phase at Various Times

$NpO_2^+$ is adsorbed when the fronts of the plumes in all three phases reach the adsorption site (**Figure 15**).

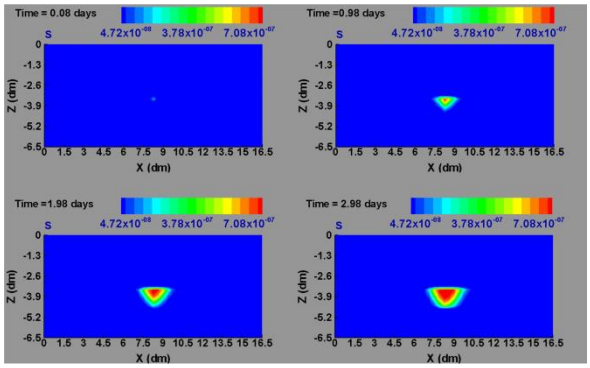


**Figure 15** Distribution of Total Adsorbed $NpO_2^+$ at Various Times

The distribution of pH is in the range of 10.50 ~ 10.71. It is seen that pH is relatively low in Region A compared to Region B **(Figure 16)**. It is further seen that pH increases along with the approach of the injected $NpO_2^+$. This is because $NpO_2^+$ and $H^+$ are competing for the same sites.

The total concentration of $CH_{4(g)}$ in the gaseous phase is shown in **Figure 17**. Although the initial and boundary conditions for $CH_{4(g)}$ are the same, the

evolution of total for $CH_{4(g)}$ is due to the complex inter-phase reactions that occur.

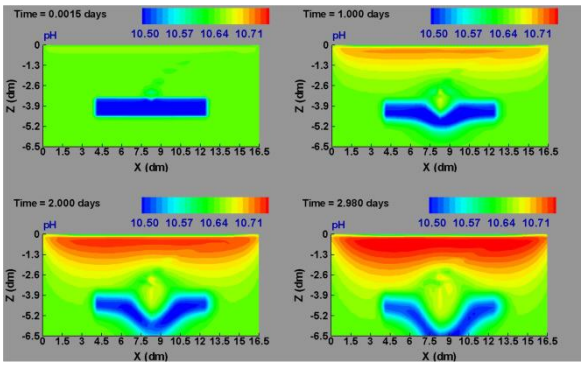


**Figure 16** Distribution of pH at Various Times

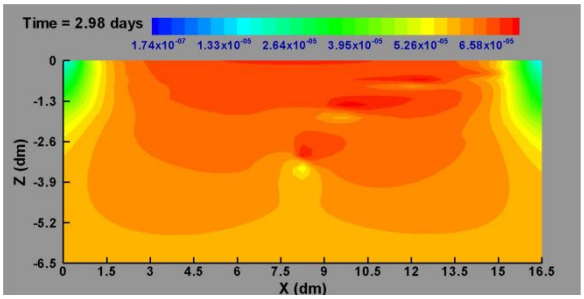


**Figure 17** Contour of Total $CH_{4(g)}$ at Time = 2.98 Days

The change in porosity results from both the boundary conditions imposed on the boundaries B2, B3, and B4, and the free displacement on boundary B1. Internal changes of pressure in all three phases, which are caused by changes in the degree of saturation and total pressure, are the major factors in the evolution of porosity (**Figure 18**).

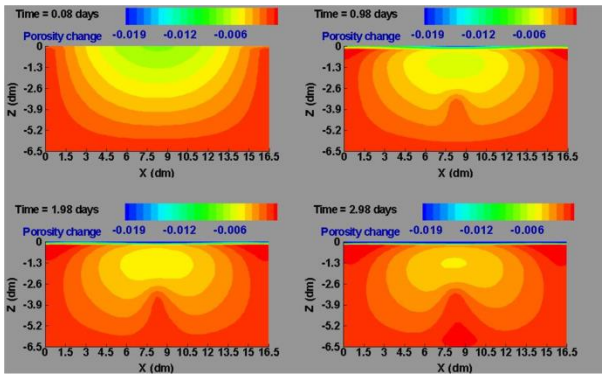


**Figure 18** Distribution of Change of Porosity at Various Times

## 4. Conclusion and Summary

The coupled groundwater processes include fluid flow in either variably saturated media or multiple phases, thermal transport, geo-mechanics, and reactive transport. Advances in the related numerical models center around their increasing design capability with regard to representing these coupled processes: from the simplest one-phase groundwater flow to the most complete of the aforementioned processes. Many fully or partially coupled THMC models or single process models have been developed for practical applications. However, current models are still incomplete, since electro-magnetic waves have not yet been coupled with THMC processes. A hypothetical example was employed in this study to illustrate simulations of fully coupled multiphase flow, thermal transport, reactive transport, and geo-mechanics. Extensive test of fully coupled THMC models is expected in the future (DECOVALEX 2019).

## 2.5 References


Abriola, L. M. and G. F. Pinder, 1985a. A multiphase approach to the modeling of porous media contamination by organic compounds, 1. Equation development. Water Resources Research 1985;21(1):11-18.

Abriola, L. M. and G. F. Pinder, 1985b. A multiphase approach to the modeling of porous media contamination by organic compounds, 2. Numerical Simulation, Water Resources Research, 1985;21(1):19-26.

Allen, M.B., 1983. Collocation techniques for modeling compositional flows in porous media. Ph.D. Dissertation. Dept. Of Civil Eng., Princeton University, Princeton, New Jersey (1983). Dept. Of Civil Eng., Princeton University, Princeton, New Jersey (1983

Burdine, N.T., 1953. Relative permeability calculations from pore-size data. Trans. A.I.M.E. 198, 71-77, 1953.

Chang, Jing-Ru C., 1995. Numerical Modeling of Three-Dimensional Subsurface Flow, Heat Transfer, and Fate and Transport of Chemicals and Microbes. PhD Dissertation. Department of Civil and Environmental Engineering, The Pennsylvania State University, University Park, PA. 253 pp.

Cheng, Hwai-Ping, 1995. Development and Application of a Three-dimensional Finite Element Model of Subsurface Flow, Heat Transfer, and Reactive Chemical Transport. PhD Dissertation. Department of Civil and Environmental Engineering, The Pennsylvania State University, University Park, PA. 357 pp.

Cheng, H. P., J. R. Cheng, and G. T. Yeh, 1998. A Lagrangian-Eulerian Method with Adaptively Local

Zooming and Peak/Valley Capturing Approach to Solve Three-Dimensional Advection-Diffusion Transport Equations. International Journal for Numerical Methods in Engineering, 41:587-615.

Chilakapati, A., T. Ginn, and J. Szecsody, 1998. An Analysis of Complex Reaction Networks in Groundwater Modeling, Water Resources Research, Vol. 34, pp. 1767-1780, 1998.

DECOVALEX 2019. DEvelopment of COupled models and their VALidation against EXperiments, 2016-2019. https://www.quintessa.org/latest-news/preparation-for-the-new-decovalex2019-project.html

Fang, F. L., G. T. Yeh, and W. D. Burgos, 2003. A New Paradigm to Model Reaction-Based Biogeochemical Processes, Water Resources Research, Vol. 39, pp. 1083-1108, 2003.

Finsterle, S, G. J. Moridis, and K. Pruess, 1994. A TOUGH2 Equation-of-State Module for the Simulation of Two-Phase Flow of Air, Water, and a Miscible Gelling Liquid. LBL-36086, UC-400. Earth Sciences Division, Lawrence Berkeley Laboratory, University of California, Berkeley, CA 94720

Guarnaccia, J. F and G. F. Pinder, 1997. NAPL: A Mathematical Model for the Study of NAPL Contamination in Granular Soils, Equation Development and Simulator Documentation. The University of Vermont, RCGRD #95-22, 1997.

Kräutle, S. and P. Knabner, 2007. A reduction scheme for coupled multicomponent transport-reaction problems in porous media: Generalization to problems with heterogeneous equilibrium reactions, Water Resources Research, Vol. 43, W03429, 2007.

Lenhard, R. J. and J. C. Parker, 1998. Experimental validation of the theory of extending two phase saturation-pressure relations to three phase systems for monotonic saturation paths, Water Resour. Res., 24, 817–830, 1988.

Liu, I-S, 2002. Continuum Mechanics, Springer-Verlag, Berlin-Heidelberg

Liu, I-S, 2006. A Continuum Mechanics Primer On Constitutive Theories of Materials. Instituto de Matematica, Universidade Federal do Rio de Janeiro, Caixa Postal 68530

Liu, I-S, R. A. Cipolatti, and M. A. Rincon, 2010. Successive linear approximation for finite elasticity. Computational and Applied Mathematics, 29(3):465–478

Liu, I-S, 2011. A note on the Mooney-Rivlin material model. Instituto de Matematica, Universidade Federal do Rio de Janeiro, 21945-970, Rio de Janeiro, Brasil

Parker, J. C., Lenhard, R. J., and T. Kuppusamy, 1987a: A parametric model for constitutive properties governing multiphase flow in porous media. Water Resour. Res., 23(4), 618--624.

Parker, J. C., and R. J. Lenhard, 1987b: A model for hysteretic constitutive relations governing multiphase flow: 1. Saturation-pressure relations. Water Resour. Res., 23(12): 2187--2196.

Pruess, K., 1991. EOS7, An equation-of-state module for the TOUGH2 simulator for two-Phase flow of saline water and air, Lawrence Berkeley Laboratory Report LBL-31114, Berkeley, CA.

Suk, H., 2003. Development of 2-D and 3-D Simulator for Three-Phase Flow with General Initial and Boundary Conditions on the Fractional Flow Approach. PhD Dissertation. The Department of Civil and Environmental Engineering, Pennsylvania State University, University Park, PA. pp. 282.

Suk, H. and G. T. Yeh, 2007. 3D, three-phase flow simulations using the Lagrangian-Eulerian approach with adaptively zooming and peak/valley capturing scheme (LEZOOMPC). Hydrologic Engineering, ASCE, 12(1): 14-32.

Tsai, C. H. and G. T. Yeh, 2012. Retention Characteristics for Systems of Multiple Phase-Fluids. Terrestrial, Atmospheric, and Oceanic Sciences (TAO), 23(4):451-458, doi:10.3319/ TAO.2012.0.14.01(Hy).

Tsai, C. H. and G. T. Yeh, 2013. An Advanced Constitutive Law in Multiphase Flow Model for Simulations in Compressible Media. Recent advances in Hydrogeology, American Geophysical Union, Chap 2, pp.27-56., 2013.

Tsai, C. H. and G. T. Yeh, 2014. Benchmarking a THMC Process Problem with an Explicitly Coupling Model in Subsurface Media. Abstract and Program, SSBench IV. Chateau de Cadarache, France, October 6 - 8, 2014. pp. 40

van Genuchten, M. Th., 1980: A closed-form equation for predicting the hydraulic conductivity of unsaturated soils, Soil Sci. Soc. Am. J., 44, 892--898.

White, M. D. and M. Oostrom, 1995. STOMP Subsurface Transport Over Multiphases. Theory Guide. PNL - XXXX. Pacific Northwest National Laboratory, Richland, WA 99352

White M. D., M. Oostrom, and R. J. Lenhard, 1995. Modeling fluid flow and transport in variably saturated porous media with the STOMP simulator. 1. Nonvolatile three-phase model description. Advances in Water Resources 1995;18(6):353-364.

Xu, T. and K. Pruess, 1998. Coupled Modeling of Non-Osothermal Multi-phase Flow, Solute Transport and Reactive Chemistry in Porous and Fractured Media: 1. Model Development and Validation. LBNL-42050. Earth Sciences Division, Lawrence Berkeley National Laboratory, Berkeley, CA 94720.

Xu, T., K. Pruess, and G. Brimhall, 1998. An Improved Equilibrium-Kinetics Speciation Algorithm for Redox Reactions in Variably Saturated Subsurface Flow Systems. LBNL-41789. Earth Sciences Division, Lawrence Berkeley National Laboratory, Berkeley, CA 94720.

Xu, T., E. Sonnenthal, N. Spycher, and Pruess, 2003. TOUGHREACT User's Guide: A Simulation Program for Non-Isothermal Multiphase Reactive Geochemical Transport in Variably Saturated Geologic Media. Berkeley: Lawrence Berkeley National Laboratory, 2003.

Yeh, G. T. and V. S. Tripathi, 1989. "A Critical Evaluation of Recent Developments in Hydrogeochemical Transport Models of Reactive Multichemical Components", Water Resources Research, vol. 25, pp. 93-108, 1989

Yeh, G. T., 1990. A Lagrangian-Eulerian method with zoomable hidden fine-mesh approach to solving advection-dispersion equations, Water Resources Res. 26(6): 1133-1144 June 1990.

Yeh G. T., J. R. Chang, H. P. Cheng, and C. H. Sung, 1995. An adaptive local grid refinement based on the exact peak capturing and oscillation free scheme to solve transport equations. Int. J. Comput. Fluids 1995;24:293-329.

Yeh, G. T. and C. H. Tsai, 2011. Proposing a New Retention Function for Multiple Phase-Fluids. Abstract and Program, 2011 AGU Fall Meeting, CD. December 5-9, 2011

Yeh, G. T. and C. H. Tsai, 2013. HYDROGEOCHEM 6.0 A Two-Dimensional Model of Coupled Fluid Flow, Thermal Transport, HYDROGEOCHEMical Transport, and Geomechanics through Multiple Phase Systems Version 6.0 (FACTM2D): Theoretical Basis and Numerical Approximation. Graduate Institute of Applied Geology, National Central University, 300 Jhongda Road, Jhongli, Taoyuan 32001

Yeh, G. T. and C. H. Tsai, 2015a. HYDROGEOCHEM 6.1: A Two-Dimensional Model of Coupled Fluid Flow, Thermal Transport, HYDROGEOCHEMical Transport, and Geomechanics through Multiple Phase Systems Version 6.1 (A Two Dimensional THMC Processes Model) Theoretical Basis and Numerical Approximation. Technical Report. Graduate Institute of Applied Geology, National Central University. DOI: 10.13140/RG.2.1.1766.2482

Yeh, G. T. and C. H. Tsai, 2015b. HYDROGEOCHEM 7.1: A Three-Dimensional Model of Coupled Fluid Flow, Thermal Transport, HYDROGEOCHEMical Transport, and Geomechanics through Multiple Phase Systems Version 7.1 (A Three Dimensional THMC Processes Model). Technical Report. Graduate Institute of Applied Geology, National Central University. DOI: 10.13140/RG.2.1.3339.1125.

Zhang, F., L. Jiang, and G. T. Yeh. 2008. An adaptive local grid refinement and peak/valley capture algorithm to solve transport problems with moving sharp-fronts J Transport in Porous Media. 72:53–69, DOI 10.1007/s11242-007-9135-2.

Table 1 List of Partially or Fully Coupled THMC Process Models

| 0 | 1 | 2 | 3 | | 4 | 5 | 6 | | 7 |
|---|---|---|---|---|---|---|---|---|---|
| | | | (H) Flow | | | | (C ) Chemical Transport[f] | | |
| No | Model | Multiple Scales Media[a] | Phase[b] | Approach[c] | (T) Thermal Transport[d] | (M) Geo-Mechanics[e] | No of Components | Component Automated? | THMC[g] included? |
| 1 | MODFLOW (USGS) | Macro | 1P | p- | None | None | N/A | N/A | H |
| 2 | GMS-FEMWATER (PSU, Army Corps) | Macro | VF | p- | None | None | 1 | N/A | HC |
| 3 | SEWAT (USGS) | Macro | VF | p- | None | None | 1 | N/A | HC |
| 4 | FEFLOW (DHI) | Macro | VF | p- | Yes | None | MS | N/A | THC |
| 5 | AT123D (ORNL, Seview) | Macro | 1p | None | None | None | 1 | N/A | C |
| 6 | PHREEQC (USGS) | Macro | none | None | None | None | MCMS | No | C(R) |
| 7 | OS3D/GIMRT (PNNL) | Macro, Fracture | 1P | p- | Input | No | MCMS | No | C(R) |
| 8 | CrunchFlow (LBNL) | Macro, Fracture | 1P | p- | Input | No | MCMS | No | THC(R) |
| 9 | NUFT-C (LLNL) | Macro, Fracture | VF | p- | Yes | No | MCMS | No | THC(R) |
| 10 | FEHM (LANL) | Marco, Fracture | 3P | p- | Yes | Solid Mech | MS | N/A | THMC |
| 11 | STORM/STOMP/ECKEChem (PNNL) | Macro, Fracture | 3P | p- | Yes | No | MCMS | No | THC(R) |
| 12 | PARSSIM1 (UT Texas) | Macro, Fracture | VF | p- | Yes | No | MCMS | No | THC(R) |
| 13 | RT3D (Auburn Univ) | Macro | 1P | input | Input | No | MS | N/A | C(R) |
| 14 | MT3D (Univ Alabama) | Macro | 1P | p- | No | No | MS | N/A | C |
| 15 | HP1/HP2/HP3 (UC Riverside ) | Macro | VF | p- | Yes | No | MS | N/A | THC(R) |
| 16 | UTCHEM | Macro | 3P | ff- | Yes | Cmp | MCSS | No | THC |
| 17 | MULTI-FLO/PFLOTRAN (LANL) | Macro, Fracture | 2P | p- | Yes | No | MCMS | No | THC(R) |
| 18 | TOUGH2/TOUGHREACT (LBNL) | Macro, Meso, Fracture | 3P | p- | Yes | Solid Mech | MCMS | No | THMC(R) |
| 19 | MIN3P (Canada) | Macro, Fracture | VF | p- | Yes | No | MCMS | No | THC(R) |
| 20 | CORE (Spain) | Macro, Fracture | 2P | p- | Yes | No | MCMS | No | THC(R) |
| 21 | COMSOL Multiphysics-PHREEQC (SKB) | Macro, Fracture | VF | p- | Yes | GeoMech | MCMS | No | THMC(R) |
| 22 | OpenGeoSys (UFZ, Germany) | Macro, Fracture | VF | p- | Yes | Solid Mech | MCMS | No | THMC(R) |
| 23 | FRACHem (Switzerland) | Fracture | 1p | p- | Yes | None | MCMS | No | THC(R) |
| 24 | HYTEC-CHESS-R2D2 (France) | Macro, Fracture | 1P | p- | Yes | No | MCMS | No | THC(R ) |
| 25 | COUPLYS (PNC, Japan) | Macro, Fracture | VF | p- | Yes | Solid Mech | MCMS | No | THMC(R) |
| 26 | THM (Korea) | Macro, Fracture | 2P | p- | Yes | GeoMech | No | No | THM |
| 27 | MURF-MURT (PSU-ORNL) | Macro, Meso, Micro, Fracture | VF | p- | No | Cmp | 1 | No | HC |
| 28 | COWADW123D (PSU) | Macro, Fracture | VF | p- | No | GeoMech | No | No | HM |
| 29 | HBGC123 (PSU - ORNL) | Macro, Meso, Micro, Fracture | VF | p- | No | Cmp | MCMS | No | C(R) |
| 30 | MPS (PSU-UCF) | Macro, Fracture | 3P | ff- | No | No | No | No | H |
| 31 | HYDROBIOGEOCHEM (PSU-UCF) | Macro, Fracture | 3P | Input | Yes | Cmp | MCMS | Yes | THC(R) |
| 32 | HYDROGEOCHEM 4.0 5.0 (UCF-ORNL) | Macro, Fracture | VF | p- | Yes | Cmp | MCMS | Yes | THC(R) |
| 33 | HGC 4.1 to 4.6 & 5.1 to 5.6 (NCU-TPC) | Macro, Fracture | VF | p- | Yes | Cmp, GeoMech | MCMS | Yes | THC(R),THMC(R) |
| 34 | HGC 6.0 to 6.2 & 7.0 to 7.2 (NCU) | Macro, Fracture | MP | ff- | Yes | GeoMech | MCMS | Yes | THMC(R) |

[a]Macro = Macroscale, Meso = Mesoscale, Micro = Microscale, Fracture = Fracture scale; [b]1P = 1 phase, VF = Variably saturated flow. 2P = 2 phases, 3P = 3 phases, MP = Multiple phase (more than 3 phases); [c]p- = Pressure-based approach, ff- = fractional flow-based approach, input = Must obtain flow field from other models; [d]Yes = modeled, no = not included, input = temperature is input parameter; [e]Cmp = Compressibility is input, geomechanics not explicitly modeled, No = not included, Solid Mech = Solid Mechanics, GeoMech = Geo-Mechanics; [f]MCMS = Multiple components-multiple species, MS = Multiple species (No concept of components), MCSS = Multiple Components-single species; gC(R) = Reaction-based Chemistry

Table 1 List of Partially or Fully Coupled THMC Process Models (Continued)

| 0 | 1 | 8 | | | | | | | 9 | | 10 |
|---|---|---|---|---|---|---|---|---|---|---|---|
| | | Geochemical Reactions[h] | | | | | | | Numerical Methods[i] | | GUI and |
| No | Model | A/C | A/D | I/E | P/D | Bio | UDA | UDR | ACRT | Transport | MeshGen |
| 1 | MODFLOW (USGS) | N/A | N/A | N/A | N/A | N/A | N/A | N/A | N/A | N/A | Yes |
| 2 | GMS-FEMWATER (PSU, Army Corps) | No | EQ | No | No | KI | N/A | N/A | N/A | FEM, LE-FEM | Yes |
| 3 | SEWAT (USGS) | No | EQ | No | No | KI | N/A | N/A | N/A | FEM | No |
| 4 | FEFLOW (DHI) | No | EQ | No | No | KI | N/A | N/A | N/A | FEM | Yes |
| 5 | AT123D (ORNL, Seview) | No | EQ | No | No | KI | N/A | N/A | N/A | Analytical | Yes |
| 6 | PHREEQC (USGS) | EQ | EQ | EQ | EK | KI | None | All | OS | Mixed Cell | Yes |
| 7 | OS3D/GIMRT (PNNL) | EQ | EQ | No | EK | No | None | None | OS, DSA(GIM), SIA | FDM | No |
| 8 | CrunchFlow (LBNL) | EQ | EQ | EQ | EK | KI | None | All | OS, DSA(GIM) | FDM/TVD | No |
| 9 | NUFT-C (LLNL) | EQ | EQ | EQ | EK | No | None | None | DSA(GIM) | IFDM | No |
| 10 | FEHM (LANL) | EQ | EQ | No | EQ | No | None | None | OS | FEM | No |
| 11 | STORM/STOMP/ECKEChem (PNNL) | EQ | EQ | No | KI | No | None | None | OS | FDM/FVM | No |
| 12 | PARSSIM1 (UT Texas) | EK | EK | EK | EK | KI | None | None | OS | FDM | No |
| 13 | RT3D (Auburn Univ) | EQ | EQ | EQ | KI | KI | None | Bio | OS | FDM | No |
| 14 | MT3D (Univ Alabama) | EQ | EQ | EQ | KI | KI | None | Bio | N/A | FDM/FVM | Yes |
| 15 | HP1/HP2/HP3 (UC Riverside ) | EQ | EQ | EQ | EK | KI | None | All | OS | FEM | Yes |
| 16 | UTCHEM (UT Austin) | No | EQ | No | EK | KI | None | None | N/A | FDM/TVD | No |
| 17 | MULTI-FLO/PFLOTRAN (LANL) | EQ | EQ | No | KI | No | None | None | OS | FDM/FEM | Yes |
| 18 | TOUGH2/TOUGHREACT (LBNL) | EQ | EQ | KI | EK | KI | None | All | OS, SIA | IFDM | Yes |
| 19 | MIN3P (Canada) | EQ | EQ | EQ | EK | KI | None | None | SIA | FVM | No |
| 20 | CORE (Spain) | EQ | EQ | No | KI | No | None | None | SIA | FEM | No |
| 21 | COMSOL Multiphysics-PHREEQC (SKB) | EQ | EQ | EQ | EK | No | None | All | OS | FEM | Yes |
| 22 | OpenGeoSys (UFZ, Germany) | EQ | EQ | EQ | EK | No | None | All | OS | FEM | Yes |
| 23 | FRACHem (Switzerland) | EQ | EQ | EQ | EK | No | None | None | OS | FEM | Yes |
| 24 | HYTEC-CHESS-R2D2 (France) | EQ | EQ | EQ | EK | No | None | None | OS, SIA | FVM | Yes |
| 25 | COUPLYS (PNC, Japan) | EQ | EQ | EQ | EK | No | None | All | OS | FEM | Yes |
| 26 | THM (Korea) | No | No | No | No | No | None | None | N/A | FEM | No |
| 27 | MURF-MURT (PSU-ORNL) | No | No | No | No | No | None | None | N/A | FEM, LE-FEM | No |
| 28 | COWADE123D (PSU) | No | No | No | No | No | None | None | N/A | FEM | No |
| 29 | HBGC123 (PSU - ORNL) | EQ | EQ | EQ | EQ | KI | None | None | SIA | FEM, LE-FEM | No |
| 30 | MPS (PSU-UCF) | No | No | No | No | No | None | None | N/A | FEM, LE-FEM | No |
| 31 | HYDROBIOGEOCHEM (PSU-UCF) | EK | EK | EK | EK | EK | All | All | OS, PC, PC-OS, SIA | FEM, LE-FEM | No |
| 32 | HYDROGEOCHEM 4.0 5.0 (UCF-ORNL) | No | No | No | No | No | None | None | OS, PC, PC-OS, SIA | FEM, LE-FEM | No |
| 33 | HGC 4.1 to 4.6 & 5.1 to 5.6 (NCU-TPC) | EK | EK | EK | EK | EK | All | All | OS, PC, PC-OS, SIA | FEM, LE-FEM | No |
| 34 | HGC 6.0 to 6.2 & 7.0 to 7.2 (NCU) | EK | EK | EK | EK | EK | All | All | OS, PC, PC-OS, SIA | FEM, LE-FEM | No |

[h]A/C = Aqueous Complexation, A/D = Adsorption-Desorption, I/E = Ion Exchange, P/D = Precipitation-Dissolution, Bio = Biomediated/Biodegradation, UDA = Allow User's Defined Algebraic Equations for Equilibrium Reactions, UDR = Allow User's Defined Rate Equations for Kinetic Reactions, KI = kinetic reaction, EK = Equilibrium or kinetic reaction, No = not modeled, EQ = Equilibrium reaction, BIO = User's defined rates are allowed only for biomediated reactions, All = User's defined rates are allowed for all reactions; [i]ACRT = Approach to Coupled Reaction and Transport, OS = Operator splitting, DSA(GIM) = Direct substitution approach(Global implicit method), PC = Predictor-corrector, SIA = Sequential iteration approach, FDM = Finite difference method, FVM = Finite volume method, IDFM = Integrated FDM, FEM = Finite element method, TVD = Total Variation Diminishing, LE-FEM = Lagrangian-Eulerian FEM.

Table 2 Reaction Network: 28 Reactions, 42 Species

| Aqueous Phase Reactions | No | Equilibrium Constants |
|---|---|---|
| $H_2O_{(l)} \leftrightarrow H^+ + OH^-$ | R1 | $\text{Log } K_1 = -14.00$ |
| $Ca^{2+} + CO_3^{2-} \leftrightarrow CaCO_{3(l)}$ | R2 | $\text{Log } K_2 = 3.22$ |
| $Ca^{2+} + H^+ + CO_3^{2-} \leftrightarrow CaHCO_3^+$ | R3 | $\text{Log } K_3 = 11.43$ |
| $Ca^{2+} \leftrightarrow H^+ + CaOH^+$ | R4 | $\text{Log } K_4 = -12.85$ |
| $H^+ + CO_3^{2-} \leftrightarrow HCO_3^-$ | R5 | $\text{Log } K_5 = 10.32$ |
| $2H^+ + CO_3^{2-} \leftrightarrow H_2CO_3$ | R6 | $\text{Log } K_6 = 16.67$ |
| $NpO_2^+ + H_2O_{(l)} \leftrightarrow H^+ + NpO_2(OH)$ | R7 | $\text{Log } K_7 = -8.85$ |
| $NpO_2^+ + CO_3^{2-} \leftrightarrow NpO_2(CO_3)^-$ | R8 | $\text{Log } K_8 = 5.60$ |
| $NpO_2^+ + 2CO_3^{2-} \leftrightarrow NpO_2(CO_3)_2^{3-}$ | R9 | $\text{Log } K_9 = -3.5$ |

| Gaseous Phase Reactions | No | Equilibrium Constants |
|---|---|---|
| $O_{(g)} + CH_{4(g)} \leftrightarrow OH_{(g)} + CH_{3(g)}$ | R10 | $\text{Log } K_{10} = -0.45$ |
| $O_{(g)} + HCO_{(g)} \leftrightarrow OH_{(g)} + CO_{(g)}$ | R11 | $\text{Log } K_{11} = 21.41$ |

| Inter Phase Isotherm Reactions | No | $S = K_d C$ |
|---|---|---|
| $NpO_{2(l)}^+ \leftrightarrow NpO_{2(NAPL)}^+$ | R12 | $K_{d,\,12} = 0.2$ |
| $NpO_{2(l)}^+ \leftrightarrow NpO_{2(g)}^+$ | R13 | $K_{d,\,13} = 0.3$ |
| $H_2O \leftrightarrow H_2O_{(NPAL)}$ | R14 | $K_{d,\,14} = 0.001$ |
| $H_2O \leftrightarrow H_2O_{(g)}$ | R15 | $K_{d,\,15} = 0.01$ |
| $NAPL \leftrightarrow NAPL_{(l)}$ | R16 | $K_{d,\,16} = 0.01$ |
| $NAPL \leftrightarrow NAPL_{(g)}$ | R17 | $K_{d,\,17} = 0.001$ |
| $Air \leftrightarrow Air_{(l)}$ | R18 | $K_{d,\,18} = 0.0001$ |
| $Air \leftrightarrow Air_{(NPAL)}$ | R19 | $K_{d,\,19} = 0.0001$ |

| Inter-phase Kinetic Reactions | No | Reaction rates |
|---|---|---|
| $H_2O \leftrightarrow H_2O_{k(NPAL)}$ | R20 | $R_{20} = 10^{-5}(H_2O) - 10^{-2}(H_2O_{k(NAPL)})$ |
| $H_2O \leftrightarrow H_2O_{k(g)}$ | R21 | $R_{21} = 10^{-5}(H_2O) - 10^{-3}(H_2O_{k(g)})$ |
| $NAPL \leftrightarrow NAPL_{k(l)}$ | R22 | $R_{22} = 10^{-5}(NAPL) - 10^{-2}(NAPL_{k(l)})$ |
| $NAPL \leftrightarrow NAPL_{k(g)}$ | R23 | $R_{23} = 10^{-5}(NAPL) - 10^{-2}(NAPL_{k(g)})$ |
| $Air \leftrightarrow Air_{k(l)}$ | R24 | $R_{24} = 10^{-5}(Air) - 10^{-1}(Air_{k(l)})$ |
| $Air \leftrightarrow Air_{k(NPAL)}$ | R25 | $R_{25} = 10^{-5}(Air) - 10^{-1}(Air_{k(NAPL)})$ |

| Adsorption-Desorption Reactions | No | Equilibrium Constants |
|---|---|---|
| $=SOH \leftrightarrow H^+ + =SO^-$ | R26 | $\text{Log } K_{26} = -10.30$ |
| $=SOH + H^+ \leftrightarrow =SOH_2^+$ | R27 | $\text{Log } K_{27} = 5.40$ |
| $NpO_2^- + H_2O + =SOH \leftrightarrow H^+ + (NpO_2)(OH)(=SOH)$ | R28 | $\text{Log } K_{28} = -3.5$ |